Influence of the Halogen in Titanocene Halide Promoted Reductions

Rasmus J. Enemærke, Jens Larsen, Gitte H. Hjøllund, Troels Skrydstrup,* and Kim Daasbjerg*

Department of Chemistry, University of Aarhus, Langelandsgade 140, 8000 Aarhus C, Denmark

Received September 24, 2004

Ti^{III} species generated in tetrahydrofuran by a Zn-based reduction of Cp_2TiX_2 (X = Cl, Br, and I) have been identified by means of cyclic voltammetry and kinetic measurements to be a mixture of Cp_2TiX, $(Cp_2TiX)_2$, and Cp_2Ti^+. The distribution of these species is found to be dependent on the halogen in that Cp_2Ti^+ is formed in quite substantial amounts for X = Br and I, but not at all for X = Cl. In all three solutions Cp_2TiX and $(Cp_2TiX)_2$ are present in appreciable amounts characterized by a dimerization equilibrium constant of $(1-3) \times 10^3$ M^{-1}. The reactivity of $(Cp_2TiX)_2$ is larger than or comparable to that of Cp_2TiX and Cp_2Ti^+, as assessed in their reactions with benzyl chloride and benzaldehyde. In addition, the rate data are essentially independent of the halogen, and no correlation is observed with the standard potentials determined in cyclic voltammetry for the different Ti^{IV}/Ti^{III}-based redox pairs. This indicates high inner-sphere character of the electron transfer processes. Analysis of the diastereoselectivities found for the hydrobenzoin formation in the titanocene chloride promoted pinacol couplings of benzaldehyde shows high *dl:meso* ratios of 97:3 with a decreasing trend as X is changed from Cl to Br and I. This effect is suggested to be due to stereoelectronic interactions between the titanocene moieties in the developing Ti^{IV}-bound pinacolate of the transition state.

Introduction

In recent years, metal-reduced titanocene dichloride, Met-Cp_2TiCl_2 (Met = Zn, Mn, and Al), has found interesting applications as selective single-electron-donating reagents, where stoichiometric amounts of the metal are employed to generate Ti^{III}-based species from reduction of Cp_2TiCl_2.[1] Such reagents have found widespread use in synthetic organic chemistry, promoting highly diastereoselective pinacol coupling reactions,[2] epoxide openings to alkyl radicals,[3] reductions of alkyl halides such as glycosyl bromides[4] and *vic*-dibromides,[5] Reformatsky additions,[6] and others.[7−9] Furthermore, interesting catalytic versions of some of the synthetic transformations have been developed, whereby Ti^{III} is regenerated in situ after electron transfer to the substrate.[1] Despite their importance, information concerning the nature and reactivity of the Ti^{III} species formed in Met-Cp_2TiCl_2 solutions has been lacking. Such information is undoubtedly crucial for the application of these reducing agents to other transformations, as well as for the design of asymmetric variants of the above reactions.[1]

Recently, we have elucidated the mechanism of the electrochemical and metal-induced reductions of Cp_2TiCl_2 in tetrahydrofuran (THF) by means of cyclic voltammetric and kinetic measurements.[10] We were able to demonstrate that the principal constituents of the Met-Cp_2TiCl_2 solutions were the monomeric Cp_2TiCl and dimeric $(Cp_2TiCl)_2$.[10] Trinuclear complexes or ionic clusters were not the reacting species in solution[11] despite their isolation and characterization in the solid phase.[12] In Chart 1, we have collected the proposed structures of Cp_2TiX (**I**), $(Cp_2TiX)_2$ (**II** and **III**), and the trinuclear complex (**IV**) using X as a symbol for the halogen and assuming that any free coordination site will be occupied by a solvent molecule, i.e., THF. The symmetric arrangement **II** of the dimer is based on an analysis of the solid-state structure,[13] and it is not known to what extent this structure in solution can be partly broken to the half-open arrangement **III** as discussed elsewhere.[10c]

One of the questions that came out of our previous studies is related to the importance of the chlorine in Met-Cp_2TiCl_2 and whether this halogen can be substituted with bromine or iodine. So far Met-Cp_2TiBr_2 and Met-Cp_2TiI_2 have not found the same extensive use as reductants as Met-Cp_2TiCl_2. Accordingly, one of the aims of the present paper is to investigate the prospects in using such systems with particular emphasis addressed at clarifying the identity of the species present, their reactivities, and the influence exerted by the

* To whom correspondence should be addressed. Fax: + 4586196199. E-mail: kdaa@chem.au.dk.

(1) (a) Gansäuer, A. *Synlett* **1998**, 801. (b) Gansäuer, A.; Bluhm, H. *Chem. Rev.* **2000**, *100*, 2771. (c) Spencer, R. P.; Schwartz, J. *Tetrahedron* **2000**, *56*, 2103. (d) Gansäuer, A. In *Radicals in Organic Synthesis*; Renaud, P., Sibi, M. P., Eds.; Wiley-VCH: Weinheim, Germany, 2001. (e) Li, J. J. *Tetrahedron* **2001**, *57*, 1. (f) Gansäuer, A.; Lauterbach, T.; Narayan, S. *Angew. Chem., Int. Ed.* **2003**, *42*, 5556.

(2) (a) Handa, Y.; Inanaga, J. *Tetrahedron Lett.* **1987**, *28*, 5717. (b) Barden, M. C.; Schwartz, J. *J. Am. Chem. Soc.* **1996**, *118*, 5484. (c) Gansäuer, A. *J. Chem. Soc, Chem. Commun.* **1997**, 457. (d) Gansäuer, A.; Moschioni, D.; Bauer, D. *Eur. J. Org. Chem.* **1998**, *1923*, 3. (e) Gansäuer, A.; Bauer, D. *J. Org. Chem.* **1998**, *63*, 2070. (f) Gansäuer, A.; Bauer, D. *Eur. J. Org. Chem.* **1998**, *2673*, 3. (g) Dunlap, M. S.; Nicholas, K. M. *Synth. Commun.* **1999**, *29*, 1097. (h) Halterman, R. L.; Zhu, C.; Chen, Z.; Dunlap, M. S.; Khan, M. A.; Nicholas, K. M. *Organometallics* **2000**, *19*, 3824. (i) Dunlap, M. S.; Nicholas, K. M. *J. Organomet. Chem.* **2001**, *630*, 125.

10.1021/om049257m CCC: $30.25
Publication on Web 02/11/2005

Chart 1. Proposed Structures of Cp_2TiX (I), $(Cp_2TiX)_2$ (II and III), and Trinuclear Complexes (IV) in THF

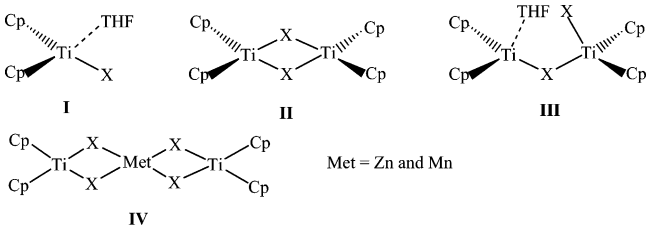

halogen on the diastereoselectivity for the hydrobenzoin formation in pinacol coupling reactions involving benzaldehyde. A detailed mechanistic investigation of the electrochemical behavior of Zn-Cp_2TiBr_2 and Zn-Cp_2TiI_2 is carried out in order to examine whether they can be encompassed in the same scheme as outlined previously for Zn-Cp_2TiCl_2.[10c] The electron-donating properties of the different Ti^{III}-based species identified are elucidated in their reactions with benzyl chloride and benzaldehyde. Finally, our study will allow us to propose how stereoelectronic effects may play an important role in controlling the diastereoselective outcome of the Met-Cp_2TiX_2-promoted pinacol coupling.

Results and Discussion

Our previous cyclic voltammetric studies of Met-Cp_2TiCl_2 in THF gave immediate access to a characterization of the redox processes shown in eqs 1−4 pertaining to the four Ti^{III}-based species $Cp_2TiCl_2^-$, $(Cp_2TiCl)_2$, Cp_2TiCl, and Cp_2Ti^+.[10]

$$Cp_2TiX_2^- - e \rightleftarrows Cp_2TiX_2 \quad (1)$$

$$(Cp_2TiX)_2 - e \rightleftarrows (Cp_2TiX)_2^+ \quad (2)$$

$$Cp_2TiX - e \rightleftarrows Cp_2TiX^+ \quad (3)$$

$$Cp_2Ti^+ - e \rightleftarrows Cp_2Ti^{2+} \quad (4)$$

A detailed analysis of the electrochemical behavior revealed that only Cp_2TiCl and $(Cp_2TiCl)_2$ were actual constituents in the solutions, whereas the other species were formed as the result of follow-up reactions occurring during the cyclic voltammetric sweep. It was also suggested that Cp_2TiCl is generated in either of the metal-induced reductions depicted in eqs 5−7, while the presence of $(Cp_2TiCl)_2$ is due to the reversible dimerization reaction depicted in eq 8, independent of the metal.

$$Zn + 2Cp_2TiX_2 \rightarrow ZnX_2 + 2Cp_2TiX \quad (5)$$

$$Mn + 2Cp_2TiX_2 \rightarrow MnX_2 + 2Cp_2TiX \quad (6)$$

$$Al + 3Cp_2TiX_2 \rightarrow AlX_3 + 3Cp_2TiX \quad (7)$$

$$2Cp_2TiX \underset{k_{-8}}{\overset{k_8}{\rightleftharpoons}} (Cp_2TiX)_2 \quad (8)$$

In the present work cyclic voltammograms of Zn-Cp_2TiBr_2 and Zn-Cp_2TiI_2 were recorded to elucidate if the mechanistic picture would be the same as for Zn-Cp_2TiCl_2. A selection of voltammograms for all three kinds of solutions is collected in Figures 1 and 2. In our previous detailed analysis of Zn-Cp_2TiCl_2 it was shown that the first broad oxidation wave appearing at ca. −0.8 V vs Fc^+/Fc (abbreviation for ferrocenium/ferrocene) splits into two waves upon increasing the sweep rate, encompassing the oxidation of both $(Cp_2TiCl)_2$ in eq 2 and Cp_2TiCl in eq 3, i.e., the two constituents in the equilibrium reaction of eq 8.[10c] These electrode processes are followed by chemical reactions, where Cp_2Ti^+ with the characteristic oxidation wave at −0.4 V vs Fc^+/Fc corresponding to eq 4 is generated either from a so-called father-son reaction involving Cp_2TiCl and Cp_2TiCl^+ or from a direct fragmentation of $(Cp_2TiCl)_2^+$ as shown in eqs 9 and 10, respectively.

(3) (a) Nugent, W. A.; RajanBabu, T. V. *J. Am. Chem. Soc.* **1988**, *110*, 8561. (b) RajanBabu, T. V.; Nugent, W. A. *J. Am. Chem. Soc.* **1989**, *111*, 4525. (c) RajanBabu, T. V.; Nugent, W. A.; Beattie, M. S. *J. Am. Chem. Soc.* **1990**, *112*, 6408. (d) Yadav, J. S.; Shekharam, T.; Gadgil, V. R. *J. Chem. Soc., Chem. Commun.* **1990**, 843. (e) Yadav, J. S.; Shekharam, T.; Srinivas, D. *Tetrahedron Lett.* **1992**, *33*, 7973. (f) RajanBabu, T. V.; Nugent, W. A. *J. Am. Chem. Soc.* **1994**, *116*, 986. (g) Maiti, G.; Roy, S. C. *J. Chem. Soc., Perkin Trans. 1* **1996**, 403. (h) Chakraborty, T. K.; Dutta, S. *J. Chem. Soc., Perkin Trans. 1* **1997**, 1257. (i) Gansäuer, A.; Pierobon, M.; Bluhm, H. *Angew. Chem., Int. Ed.* **1998**, *37*, 101. (j) Gansäuer, A.; Bluhm, H. *J. Chem. Soc, Chem. Commun.* **1998**, 2143. (k) Gansäuer, A.; Bluhm, H.; Pierobon, M. *J. Am. Chem. Soc.* **1998**, *120*, 12849. (l) Mandal, P. K.; Maiti, G.; Roy, S. C. *J. Org. Chem.* **1998**, *63*, 2829. (m) Gansäuer, A.; Lauterbach, T.; Bluhm, H.; Noltemeyer, M. *Angew. Chem., Int. Ed.* **1999**, *38*, 2909. (n) Fernández-Mateos, A.; Martín de la Nava, E.; Coca, G. P.; Silvo, A. R.; González, R. R. *Org. Lett.* **1999**, *1*, 607. (o) Gansäuer, A.; Pierobon, M. *Synlett* **2000**, 1357. (p) Chakraborty, T. K.; Das, S. *Chem. Lett.* **2000**, 80. (q) Rana, K. K.; Guin, C.; Roy, S. C. *Tetrahedron Lett.* **2000**, *41*, 9337. (r) Gansäuer, A.; Bluhm, H.; Pierobon, M.; Keller, M. *Organometallics* **2001**, *20*, 914. (s) Gansäuer, A.; Pierobon, M.; Bluhm, H. *Synthesis* **2001**, 2500. (t) Gansäuer, A.; Bluhm, H.; Lauterbach, T. *Adv. Synth. Catal.* **2001**, *343*, 785. (u) Chakraborty, T. K.; Tapadar, S. *Tetrahedron Lett.* **2001**, *42*, 1375. (v) Chakraborty, T. K.; Das, S.; Raju, T. V. *J. Org. Chem.* **2001**, *66*, 4091. (w) Hardouin, C.; Chevallier, F.; Rousseau, B.; Doris, E. *J. Org. Chem.* **2001**, *66*, 1046. (x) Gansäuer, A.; Rinker, B. *Tetrahedron* **2002**, *58*, 7017. (y) Chakraborty, T. K.; Das, S. *Tetrahedron Lett.* **2002**, *43*, 2313. (z) Parrish, J. D.; Little R. D. *Org. Lett.* **2002**, *4*, 1439. (aa) Barrero, A. F.; Oltra, J. E.; Cuerva, J. M.; Rosales, A. *J. Org. Chem.* **2002**, *67*, 2566. (bb) Gansäuer, A.; Rinker, B.; Pierobon, M.; Grimme, S.; Gerenkamp, M.; Mück-Lichtenfeld, C. *Angew. Chem., Int. Ed.* **2003**, *42*, 3687. (cc) Anaya, J.; Fernández-Matos, A.; Grande, M.; Martiánez, J.; Ruano, G.; Rubio-González R. *Tetrahedron* **2003**, *59*, 241. (dd) Ruano, G.; Martiánez, J.; Grande, M.; Anaya, J. *J. Org. Chem.* **2003**, *68*, 2024. (ee) Barrero, A. F.; Rosales, A.; Cuerva, J. M.; Oltra, J. E. *Org. Lett.* **2003**, *5*, 1935. (ff) Gansäuer, A.; Pierobon, M.; Bluhm, H. *Angew. Chem., Int. Ed.* **2002**, *41*, 3206. (gg) Justicia, J.; Rosales, A.; Buñuel, E.; Oller-López, J. L.; Valdivia, M.; Haïdour, A.; Oltra, J. E.; Barrero, A. F.; Cárdenas, D. J.; Cuerva, J. M. *Chem. Eur. J.* **2004**, *10*, 1778. (hh) Fernández-Mateos, A.; Mateos Burón, L.; Rabanedo Clemente, R.; Ramos Silvo, Ana I.; Rubio González, R. *Synlett* **2004**, 1011.

(4) (a) Cavallaro, C. L.; Schwartz, J. *J. Org. Chem.* **1995**, *60*, 7055. (b) Spencer, R. P.; Schwartz, J. *Tetrahedron Lett.* **1996**, *37*, 4357. (c) Spencer, R. P.; Schwartz, J. *J. Org. Chem.* **1997**, *62*, 4204. (d) Spencer, R. P.; Cavallaro, C. L.; Schwartz, J. *J. Org. Chem.* **1999**, *64*, 3987. (e) Hansen, T.; Krintel, S. L.; Daasbjerg, K.; Skrydstrup, T. *Tetrahedron Lett.* **1999**, *40*, 6087. (f) Hansen, T.; Daasbjerg, K.; Skrydstrup, T. *Tetrahedron Lett.* **2000**, *41*, 8645.

(5) Davies, S. G.; Thomas, S. E. *Synthesis* **1984**, 1027.

(6) Parrish, J. D.; Shelton, D. R.; Little, R. D. *Org. Lett.* **2003**, *5*, 3615.

(7) Russo, T.; Pinhas, A. R. *Organometallics* **1999**, *18*, 5344.

(8) Zhou, L.; Hirao, T. *Tetrahedron* **2001**, *57*, 6927.

(9) Barrero, A. F.; Rosales, A.; Cuerva, J. M.; Gansäuer, A.; Oltra, J. E. *Tetrahedron Lett.* **2003**, *44*, 1079.

(10) (a) Enemærke, R. J.; Hjøllund, G. H.; Daasbjerg, K.; Skrydstrup, T. *C. R. Acad. Sci.* **2001**, *4*, 435. (b) Enemærke, R. J.; Larsen, J.; Skrydstrup, T.; Daasbjerg, K. *Organometallics* **2004**, *23*, 1866. (c) Enemærke, R. J.; Larsen, J.; Skrydstrup, T.; Daasbjerg, K. *J. Am. Chem. Soc.* **2004**, *126*, 7853.

(11) For a discussion of trinuclear complexes in solution, see ref 10c and references therein.

(12) (a) Sekutowski, D. J.; Stucky, G. D. *Inorg. Chem.* **1975**, *14*, 2192. (b) Sekutowski, D.; Jungst, R.; Stucky, G. D. *Inorg. Chem.* **1978**, *17*, 1848.

(13) Coutts, R. S. P.; Wailes, P. C.; Martin, R. L. *J. Organomet. Chem.* **1973**, 375.

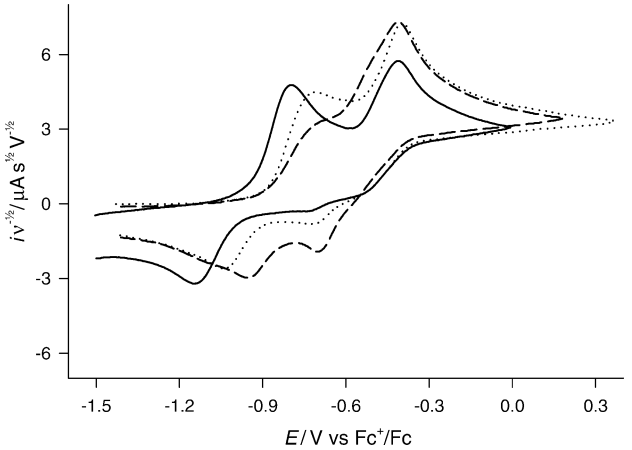

Figure 1. Cyclic voltammograms of 2 mM Zn-Cp_2TiCl_2 (—),[10c] 2.2 mM Zn-Cp_2TiBr_2 (· · ·), and 2.2 mM Zn-Cp_2TiI_2 (- - -) recorded at a sweep rate of 0.1 V s^{-1} in 0.2 M Bu_4NPF_6/THF. Currents are normalized with respect to sweep rate.

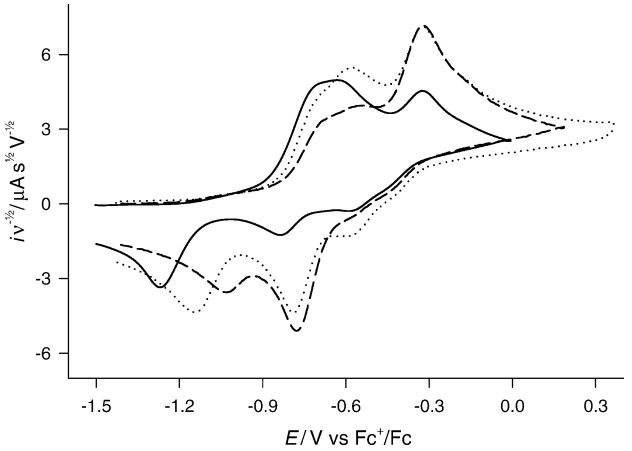

Figure 2. Cyclic voltammograms of 2 mM Zn-Cp_2TiCl_2 (—),[10c] 2.2 mM Zn-Cp_2TiBr_2 (· · ·), and 2.2 mM Zn-Cp_2TiI_2 (- - -) recorded at a sweep rate of 10 V s^{-1} in 0.2 M Bu_4NPF_6/THF. Currents are normalized with respect to sweep rate.

$$Cp_2TiX + Cp_2TiX^+ \underset{k_{-9}}{\overset{k_9}{\rightleftharpoons}} Cp_2Ti^+ + Cp_2TiX_2 \quad (9)$$

$$(Cp_2TiX)_2^+ \underset{k_{-10}}{\overset{k_{10}}{\rightleftharpoons}} Cp_2Ti^+ + Cp_2TiX_2 \quad (10)$$

The major peak present on the reverse sweep at ca. −1.2 V vs Fc$^+$/Fc originates from the reduction of Cp_2TiCl_2 (see eq 1) produced in the two above reactions. Thus, one of the main conclusions from these studies is that Cp_2Ti^+ and Cp_2TiCl_2 in contrast to Cp_2TiCl and $(Cp_2TiCl)_2$ are not present initially in the Zn-Cp_2TiCl_2 solution.

The voltammograms pertaining to Zn-Cp_2TiBr_2 and Zn-Cp_2TiI_2 show clear resemblances to those of Zn-Cp_2TiCl_2. First of all, the peak at ca. −0.4 V vs Fc$^+$/Fc coincides in all cases, independent of X, which proves that the generation of Cp_2Ti^+ is a general feature of these systems. For the broad oxidation wave appearing in the range from −0.8 to −0.5 V vs Fc$^+$/Fc, on the other hand, there is a distinct dependence on the nature of X. In analogy with the interpretation of the Zn-Cp_2TiCl_2 case, this feature is attributed to the presence of two

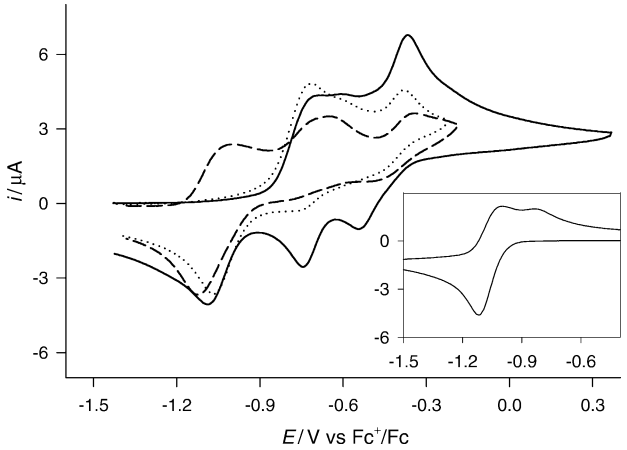

Figure 3. Cyclic voltammograms of 2.2 mM solutions of Zn-Cp_2TiBr_2 (—), Mn-Cp_2TiBr_2 (· · ·), and Al-Cp_2TiBr_2 (- - -) recorded at a sweep rate of 1.0 V s^{-1} in 0.2 M Bu_4NPF_6/THF. Inset: Cyclic voltammogram of 2 mM Cp_2TiBr_2 recorded at a sweep rate of 1.0 V s^{-1} in 0.2 M Bu_4NPF_6/THF.

electrode processes with the first wave (appearing at the most negative potential) assigned to the oxidation of $(Cp_2TiX)_2$ and the second one to the oxidation of Cp_2TiX. The presence of the dimerization equilibrium reaction involving these two species in eq 8 is revealed by the fact that the ratio of the currents for the first and second peak increases with a lowering of the sweep rate (compare Figures 1 and 2) and/or an increase of the concentration. Because of the dynamic nature of the cyclic voltammetric technique and the fact that the dimer is easier to oxidize than the monomer, it is possible to let most of the oxidation process go through the dimer at low sweep rate. Upon increasing the sweep rate, it becomes harder for the equilibrium reaction to keep up, and accordingly much more of the oxidation will go through the monomer. In that instance, the electrochemical response provides a better picture of the actual composition of the solution. As it was the case for Zn-Cp_2TiCl_2, the wave of Cp_2Ti^+ decreases relative to the wave(s) of $(Cp_2TiX)_2$ and Cp_2TiX as the sweep rate is increased and/or the concentration is lowered. This supports the interpretation that Cp_2Ti^+ is generated during the sweep because of the follow-up reactions occurring in eqs 9 and 10. However, a closer examination of the peak current ratios reveals that this tendency is less pronounced for X = Br and I than Cl, providing a first indication that there are differences in the equilibrium distribution of the Ti^{III}-based species for different X.

To reveal if the metal employed in the reduction of Cp_2TiX_2 should have any influence on the composition of the solutions, cyclic voltammograms of Zn-Cp_2TiX_2, Mn-Cp_2TiX_2, Al-Cp_2TiX_2, and Cp_2TiX_2 (X = Br and I) were recorded as shown in Figures 3 and 4. As seen, the oxidation peak potentials attributed to $(Cp_2TiX)_2$ and Cp_2TiX are independent of the metal, which indicate that trinuclear complexes involving a central metal atom are not present in either of these solutions (see **IV** in Chart 1). For Al-Cp_2TiBr_2 and Al-Cp_2TiI_2 an additional peak is apparent at ca. −1.0 and −0.9 V vs Fc$^+$/Fc, respectively, which we assign to the oxidation of $Cp_2TiBr_2^-$ and $Cp_2TiI_2^-$, respectively, consistent with the cyclic voltammograms recorded of authentic samples

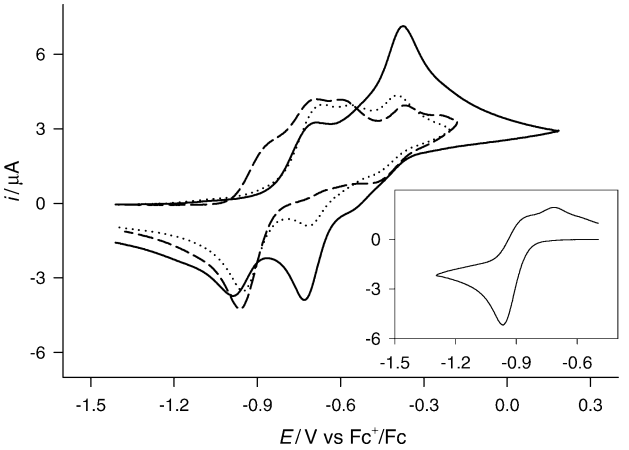

Figure 4. Cyclic voltammograms of 2.2 mM solutions of Zn-Cp_2TiI_2 (—), Mn-Cp_2TiI_2 (• • •), and Al-Cp_2TiI_2 (- - -) recorded at a sweep rate of 1.0 V s^{-1} in 0.2 M Bu_4NPF_6/THF. Inset: Cyclic voltammogram of 2 mM Cp_2TiI_2 recorded at a sweep rate of 1.0 V s^{-1} in 0.2 M Bu_4NPF_6/THF.

of Cp_2TiBr_2 and Cp_2TiI_2 (see insets of Figures 3 and 4). Exactly the same phenomenon was observed for a solution of Al-Cp_2TiCl_2, in which an oxidation wave pertaining to $Cp_2TiCl_2^-$ was detectable, although to a smaller extent.[10c] The broad oxidation wave appearing on the reverse sweep in the voltammogram of Cp_2TiI_2 encompasses both the oxidation of $Cp_2TiI_2^-$ and the $Cp_2TiI/(Cp_2TiI)_2$ system formed upon fragmentation of iodide from $Cp_2TiI_2^-$ as reported elsewhere.[10b] Even in the voltammogram of Cp_2TiBr_2 small oxidation waves of $Cp_2TiBr/(Cp_2TiBr)_2$ are detectable on the reverse sweep along with the distinct $Cp_2TiBr_2^-$ peak; these waves become more pronounced upon increasing the sweep rate.[10b]

The influence of the metal halides formed in eqs 5−7 pertains mainly to their involvement in halide transfer reactions. The halide abstraction proceeds with greater ease from aluminum halides compared to zinc and manganese halides, since the peak originating from the oxidation of $Cp_2TiX_2^-$ can only be observed in the former case. This observation is surprising, as aluminum halides are the stronger Lewis acids, although it is not known to what extent a coordination between the metal halides and THF may affect the reactivities. At the same time the presence of these chemical reactions explains why the peaks of the $Cp_2TiX_2/Cp_2TiX_2^-$ redox couple for the different Met-Cp_2TiX_2 solutions are not completely coincident with those observed for Cp_2TiX_2 and why there is a variation in the relative currents of the oxidation waves. The transformation of any of the $(Cp_2TiX)_2$, Cp_2TiX, and Cp_2Ti^+ species into $Cp_2TiX_2^-$ in cyclic voltammetry is facilitated by the presence of X^-. For instance, addition of tetrabutylammonium iodide to a Zn-Cp_2TiI_2 solution makes the voltammogram resemble that recorded for a sample of Cp_2TiI_2 (see the Supporting Information). This does not mean that $Cp_2TiI_2^-$ actually is present in the Zn-Cp_2TiI_2 solution but rather that it is formed at the electrode surface during the sweep.[10b]

On the basis of the apparent mechanistic similarities for the electrochemical behavior of the different Met-Cp_2TiX_2 solutions, we propose that a common reaction scheme, a so-called mesh scheme, can be set up as shown in Scheme 1.[10c,14] In the Supporting Information, detailed versions of this scheme are provided for Zn-Cp_2TiBr_2 and Zn-Cp_2TiI_2. The mesh scheme incorporates the four relevant electrochemical processes, eqs 1−4, along with a number of chemical reactions, including eqs 8−10. In particular, the equilibrium reactions involving $Cp_2TiX_2^-$, Cp_2TiX, $(Cp_2TiX)_2$, and Cp_2Ti^+ are important, as they determine the actual composition of the solution, while the associated rate constants are essential parameters for describing the compositional changes occurring at the electrode surface during a sweep. The oxidation of both Cp_2TiX and $(Cp_2TiX)_2$ leads ultimately to the formation of Cp_2Ti^+ and Cp_2TiX_2 because Cp_2TiX^+ reacts rapidly with Cp_2TiX or with metal halides and $(Cp_2TiX)_2^+$ fragmentates. However, at high sweep rates peaks corresponding to the reduction of Cp_2TiX^+ and $(Cp_2TiX)_2^+$ can be monitored in the cyclic voltammograms. Likewise, the absence at low sweep rates of a cyclic voltammetric reduction wave pertaining to Cp_2Ti^{2+} formed upon oxidation of Cp_2Ti^+ in eq 4 suggests that Cp_2Ti^{2+} will abstract halides from the metal halides to afford Cp_2TiX_2. The lack of the $Cp_2TiX_2^-$ oxidation wave in double sweep experiments for Met = Zn and Mn indicates that the halide transfer reactions may go the other way around also; that is, the metal halides can abstract a halide effectively from $Cp_2TiX_2^-$ produced upon the electrochemical reduction of Cp_2TiX_2 in eq 1. In general, Ti^{IV}- but not Ti^{III}-based species thus are capable of abstracting halides from the metal halides with the Al-Cp_2TiX_2 system presenting a notable exception, as the $Cp_2TiX_2^-$ wave in this case is observable.

In the further analysis of the cyclic voltammograms the goal was to obtain quantitative information about the composition of the solutions. The focus was mainly on Zn-Cp_2TiBr_2 and Zn-Cp_2TiI_2, since the voltammograms in these cases were the ones being least influenced by halide transfer reactions. This simplifies the mechanistic scheme and makes the analysis less uncertain. In general, all relevant potentials, heterogeneous and homogeneous rate constants, and equilibrium constants have been extracted by digital simulations of the experimentally obtained voltammograms recorded at different sweep rates of 0.1−50 V s^{-1} and concentrations of 1.0−2.2 mM. All simulations and fittings were carried out using the program DigiSim 3.03.[15] For such measurements, it is important that the number of experimental observations is large to diminish the overall uncertainty. In addition, the whole collection of voltammograms recorded for each solution has been simulated simultaneously to obtain the most consistent set of results. A complete and detailed description of the exact model parameters used, a discussion of the uncertainties associated with the procedure, as well as relevant fits can be found in the Supporting Information.

(14) Usually the presence of at least three redox states as well as chemical states would be required for describing such a mechanism by a mesh scheme. Thus, in the present case one might argue that the mechanistic scheme is of the ladder type, if the $(Cp_2TiX)_2^+$ species with its combination of Ti^{III} and Ti^{IV} atoms is not considered as representing a distinct redox state (see also: Evans, D. H. *Chem. Rev.* **1990**, *90*, 739).

(15) Rudolph, M.; Feldberg, S. W. *DigiSim version 3.03*; Bioanalytical Systems, Inc.: West Lafayette, IN.

Scheme 1. Mesh Scheme Describing the Reaction Mechanism for the Electrode Reactions of Met-Cp_2TiX_2 (Met = Zn, Mn, and Al; X = Cl, Br, and I) in THF

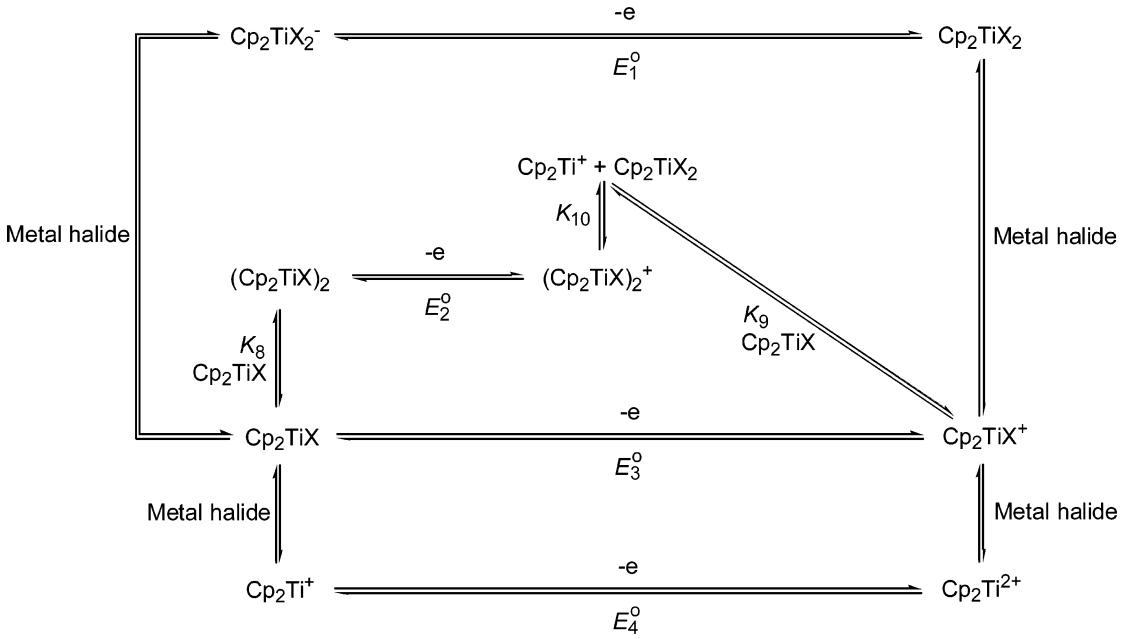

Table 1. Relevant Data Extracted from Cyclic Voltammograms Recorded on Zn-Cp_2TiX_2 Solutions[a]

	Zn-Cp_2TiCl_2 [b]	Zn-Cp_2TiBr_2	Zn-Cp_2TiI_2
E_1°/V vs Fc/Fc^+ [c]	-1.20 ± 0.03	-1.10 ± 0.05	-0.95 ± 0.05
E_2°/V vs Fc/Fc^+ [c]	-0.81 ± 0.03	-0.76 ± 0.05	-0.75 ± 0.05
E_3°/V vs Fc/Fc^+ [c]	-0.75 ± 0.03	-0.69 ± 0.05	-0.67 ± 0.05
E_4°/V vs Fc/Fc^+ [c]	-0.43 ± 0.03	-0.45 ± 0.05	-0.43 ± 0.05
$k_{s,1}$/cm s^{-1}	0.04	0.06	0.04
$k_{s,2}$/cm s^{-1}	0.02	0.015	0.015
$k_{s,3}$/cm s^{-1}	0.008	0.006	0.008
$k_{s,4}$/cm s^{-1}	0.015	0.007	0.007
K_8/M^{-1}	$3\ (2-5) \times 10^3$	$1\ (0.5-3) \times 10^3$	$1\ (0.5-3) \times 10^3$
$k_8/M^{-1}\ s^{-1}$	$2\ (1-10) \times 10^4$	$2\ (1-5) \times 10^5$	$5\ (2-10) \times 10^5$
k_{-8}/s^{-1}	6.7 (2−50)	$2\ (1-5) \times 10^2$	$5\ (2-10) \times 10^2$
K_9 [d]	3.2×10^7	1.6×10^7	2.4×10^7
$k_9/M^{-1}\ s^{-1}$	$<5 \times 10^3$	$1\ (0.5-2) \times 10^4$	$2\ (1-4) \times 10^3$
$k_{-9}/M^{-1}\ s^{-1}$	$<1.6 \times 10^{-4}$	$6.3\ (3.2-13) \times 10^{-4}$	$8.3\ (4.2-17) \times 10^{-5}$
K_{10}/M	$1\ (0.01-10^5) \times 10^3$	$1\ (0.01-10^5) \times 10^3$	$1\ (0.01-10^5) \times 10^3$
k_{10}/s^{-1}	$3\ (1-50) \times 10^2$	$3\ (1-10^2) \times 10^2$	$3\ (1-10^2) \times 10^2$
$k_{-10}/M^{-1}\ s^{-1}$	$0.3\ (10^{-5}-30)$	$0.3\ (10^{-6}-10)$	$0.3\ (10^{-6}-10)$

[a] The tabulated values are the ones providing the best fits, while those given in parentheses describe the intervals of tolerance, as determined from a manual adjustment of the parameters. To minimize the number of adjustable parameters, the uncertainties on the k_s values were not determined, but in general they can be assumed to be on the order of 50%. [b] From ref 10c. [c] Standard potentials are defined as reduction potentials and can be converted to SCE by adding 0.52 V. [d] Calculated automatically by the DigiSim program from a thermochemical cycle.

The essential data extracted from the simulation procedure are collected in Table 1 together with those obtained previously for X = Cl. A couple of points are worth noting. First of all, the agreement with the corresponding values obtained from the electrochemical reduction of Cp_2TiX_2 is good.[10b] For a given X the order of standard potentials, E°, for the four Ti-containing redox couples is as follows: $Cp_2TiX_2/Cp_2TiX_2^- \ll (Cp_2TiX)_2^+/(Cp_2TiX)_2 < Cp_2TiX^+/Cp_2TiX \ll Cp_2Ti^{2+}/Cp_2Ti^+$; that is, from a thermodynamic point of view $Cp_2TiX_2^-$ is expected to be a much stronger electron donor than Cp_2Ti^+. For a given Ti-based redox couple a relatively weak halogen effect is observed as E° increases slightly in the order X = Cl, Br, and I; that is, Cp_2TiI would be expected on this basis to be a slightly weaker electron donor than Cp_2TiCl. The halogen effect is largest for the Cp_2TiX_2 series as the difference in standard potentials going from X = Cl to I constitutes 250 mV. In general, it may be concluded that the electronic influence on the titanium nucleus is smallest, when the ligand is the larger iodide than chloride.

The heterogeneous rate constants, k_s, associated with the four electrode processes are in the range 0.006−0.06 cm s^{-1}. With respect to the equilibrium reaction in eq 8, relatively large differences are seen in the dimerization rate constant k_8 as well as k_{-8}, although the equilibrium constant K_8 is essentially independent of X: $k_8 = 2 \times 10^4\ M^{-1}\ s^{-1}$ for X = Cl, $k_8 = 2 \times 10^5\ M^{-1}\ s^{-1}$ for X = Br, and $k_8 = 5 \times 10^5\ M^{-1}\ s^{-1}$ for X = I. The large values of k_{-8} for X = Br and I are the origin of the significant appearance of Cp_2TiX in the cyclic voltammograms of Zn-Cp_2TiX_2 in these cases (see Figures 1 and 2). For the father-son reaction between Cp_2TiX and Cp_2TiX^+ in eq 9 and for the fragmentation reaction of $(Cp_2TiX)_2^+$ in eq 10 the rate constants are found to be largely independent of X. On the other hand, the

Table 2. Equilibrium Concentrations of the Ti^{III}-Based Species Present in 2 mM Solutions of Zn-Cp_2TiX_2 and Electrochemically Reduced Cp_2TiX_2 [a]

	$[Cp_2TiX_2^-]$	$[Cp_2TiX]$	$[(Cp_2TiX)_2]$	$[Cp_2Ti^+]$
X = Cl	0.00 (1.35)	0.50 (0.21)	0.75 (0.22)	0.00 (0.00)
X = Br	0.00 (0.11)	0.68 (0.39)	0.47 (0.75)	0.38 (0.00)
X = I	0.00 (0.02)	0.60 (0.40)	0.37 (0.79)	0.66 (0.00)

[a] Values for the electrochemically reduced solutions of Cp_2TiX_2 are given in parentheses, from ref 10b.

reactivity of Cp_2TiX^+ and Cp_2Ti^{2+} toward the zinc halides decreases in the order X = Cl, Br, and I as envisioned by the pronounced presence of the reduction peaks of these two species in the voltammograms of Zn-Cp_2TiBr_2 and in particular Zn-Cp_2TiI_2 (see the Supporting Information).

On the basis of the equilibrium constants extracted for the different reactions involving $Cp_2TiX_2^-$, $(Cp_2TiX)_2$, Cp_2TiX, and Cp_2Ti^+, it is possible to determine the actual composition for any of the systems studied. In Table 2 the distribution is collected for 2 mM solutions of Zn-Cp_2TiX_2 along with corresponding data evaluated for electrochemically reduced Cp_2TiX_2.[10b] The most interesting result provided by the new data pertaining to Zn-Cp_2TiBr_2 and Zn-Cp_2TiI_2 as compared with Zn-Cp_2TiCl_2 is the existence of Cp_2Ti^+ in substantial concentrations of 0.38 and 0.66 mM, respectively. The concentrations of Cp_2TiX and $(Cp_2TiX)_2$ are of the same magnitude, while there will be no $Cp_2TiX_2^-$ at all, as X^- is bound in the metal halides.[16] To account for the presence of Cp_2Ti^+ in the cases of X = Br and I, eq 5 has to be extended as shown in eq 11.

$$ZnX_2 + 2Cp_2TiX \rightleftarrows ZnX_4^{2-} + 2Cp_2Ti^+ \ (X = Br \text{ and } I) \quad (11)$$

The electrochemical reduction of Cp_2TiX_2 is characterized by the absence of metal halides, and under these conditions an equilibrium mixture of Cp_2TiX and $(Cp_2TiX)_2$ is formed for all X with no indication of Cp_2Ti^+ as seen for Zn-Cp_2TiBr_2 and Zn-Cp_2TiI_2. Moreover, for X = Cl the main constituent actually becomes $Cp_2TiCl_2^-$ (see Table 2). Thus, it may be concluded that the presence of zinc halides in the Zn-Cp_2TiX_2 solutions favors the generation of the more halogen-deficient Ti^{III} species, and as the titanium−halogen bond becomes weaker in the order X = Cl, Br and I,[17] this trend is getting more pronounced.

Kinetic Studies

With the aim of describing the reactivity of the different Ti^{III}-based species, kinetic studies were carried out on reactions involving the two electron acceptors benzyl chloride, BnCl, and benzaldehyde, PhCHO. The kinetic situation is quite complex, as the Zn-Cp_2TiX_2 solution consists of an equilibrium mixture of Cp_2TiX, $(Cp_2TiX)_2$, and Cp_2Ti^+ for X = Br and I as evaluated in Table 2. In our previous study concerning Zn-Cp_2TiCl_2, the task was simpler due to the absence of Cp_2Ti^+. In that case the reactivity of the two main constituents, Cp_2TiCl and $(Cp_2TiCl)_2$, could be extracted from the knowledge of K_8 and the associated rate constants by analyzing the changes observed in the kinetics upon varying the concentration.[10c] In addition, we succeeded in generating solutions of pure Cp_2Ti^+ [by reacting $TlPF_6$ with the $Cp_2TiCl/(Cp_2TiCl)_2$ mixture][10c] and essentially pure $Cp_2TiCl_2^-$ (by adding tetrabutylammonium chloride to an electrochemically reduced solution of Cp_2TiCl_2),[10b] thus giving access to the relevant rate parameters of these species.

Our analysis presented herein will therefore be based on the very same reaction scheme as elucidated in the Zn-Cp_2TiCl_2 case,[10c] including now the reactions pertaining to Cp_2Ti^+. The overall decay of the different Ti^{III} species and the concomitant build-up of Ti^{IV} species were followed by UV−vis spectroscopy using different initial concentrations of Zn-Cp_2TiX_2 (X = Br and I) and excess substrate. The relevant kinetic information was extracted employing the simulation program Gepasi 3.21.[18]

Benzyl Chloride. In Figures 5 and 6, some kinetic traces are collected for different concentrations of Zn-Cp_2TiBr_2 and Zn-Cp_2TiI_2 in the presence of excess BnCl. The overall kinetics exhibit a weak concentration dependency, because of the influence from the equilibrium reactions. The mechanistic basis for carrying out the fitting procedure consists of eqs 8 and 11−18, which include all relevant reactions involving Cp_2TiX, $(Cp_2TiX)_2$, and Cp_2Ti^+.[10c]

$$Cp_2TiX + BnCl \xrightarrow{k_{12}} [Cp_2TiX^+ + Cl^- + Bn^\bullet] \rightarrow Cp_2TiXCl + Bn^\bullet \quad (12)$$

$$Cp_2TiX + Bn^\bullet \rightarrow [Cp_2TiX^+ + Bn^-] \rightarrow Cp_2TiXBn \quad (13)$$

$$(Cp_2TiX)_2 + BnCl \xrightarrow{k_{14}} [(Cp_2TiX)_2^+ + Cl^- + Bn^\bullet] \rightarrow Cp_2TiX + Cp_2TiXCl + Bn^\bullet \quad (14)$$

$$(Cp_2TiX)_2 + Bn^\bullet \rightarrow [(Cp_2TiX)_2^+ + Bn^-] \rightarrow Cp_2TiX + Cp_2TiXBn \quad (15)$$

$$Cp_2Ti^+ + BnCl \xrightarrow{k_{16}} [Cp_2Ti^{2+} + Cl^- + Bn^\bullet] \rightarrow Cp_2TiCl^+ + Bn^\bullet \xrightarrow{\text{Metal halide}} Cp_2TiXCl + Bn^\bullet \quad (16)$$

$$Cp_2Ti^+ + Bn^\bullet \rightarrow [Cp_2Ti^{2+} + Bn^-] \rightarrow Cp_2TiBn^+ \xrightarrow{\text{Metal halide}} Cp_2TiXBn \quad (17)$$

$$Cp_2TiXBn + BnCl \rightarrow Cp_2TiXCl + Bn_2 \quad (18)$$

In the actual electron transfer steps between Cp_2TiX, $(Cp_2TiX)_2$, or Cp_2Ti^+ and BnCl depicted in eqs 12, 14, and 16 the benzyl radical, $Bn^\bullet$, is formed along with chloride. Chloride will be captured immediately by Cp_2TiX^+, $(Cp_2TiX)_2^+$, or Cp_2Ti^{2+} to afford Cp_2TiXCl (besides Cp_2TiX in eq 14), as revealed by the cyclic voltammetric

(16) As shown in our previous paper[10b] $Cp_2TiCl_2^-$ can be made the main constituent in any of the Met-Cp_2TiCl_2 solutions upon addition of tetrabutylammonium chloride.

(17) *Handbook of Chemistry and Physics*, 72nd ed.; Lide, D. R., Ed.; CRC Press: Boca Raton, 1991.

(18) Mendes, P. *Gepasi*, version 3.21; Virginia Tech: Blacksburg, VA, 1996−1999. The program may be downloaded from the Internet at http://www.gepasi.org.

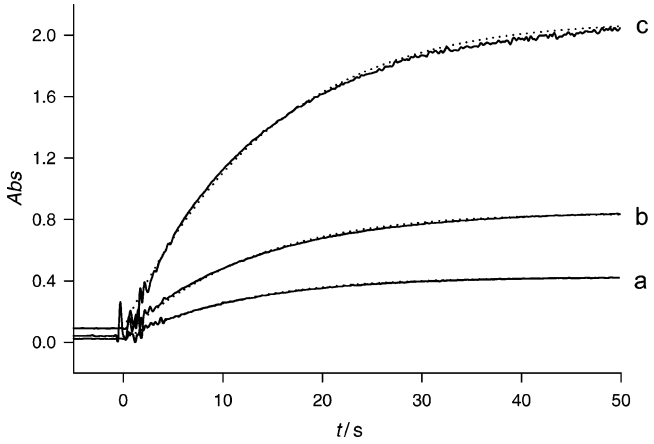

Figure 5. Kinetic traces (absorption vs time) recorded for the buildup of Ti^{IV} at a wavelength $\lambda = 535$ nm in THF for the reactions of 87 mM BnCl with (a) 1.0, (b) 2.0, and (c) 5.0 mM solutions of Zn-Cp_2TiBr_2. The dotted curves are the best fits based on simulation of eqs 8 and 11−17.

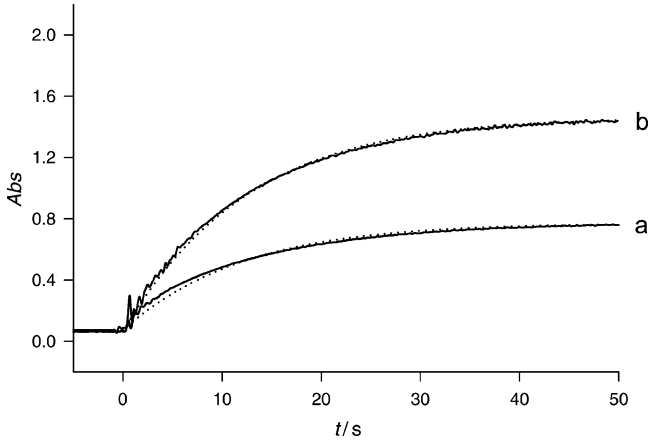

Figure 6. Kinetic traces (absorption vs time) recorded for the buildup of Ti^{IV} at a wavelength $\lambda = 535$ nm in THF for the reactions of 87 mM BnCl with (a) 1.0 and (b) 2.0 mM solutions of Zn-Cp_2TiI_2. The dotted curves are the best fits based on simulation of eqs 8 and 11−17.

analysis. Note that in eq 16 additional halide transfer from the metal halides is included to account for the formation of this product. In principle, the electron transfer and the chloride transfer might take place concertedly, which is the reason for showing the initial products within brackets. $Bn^{\bullet}$ is further reduced to the benzyl anion, Bn^-, in a fast second electron transfer process shown in eqs 13, 15, and 17, and as this anion is expected to be a strong ligand, we suggest that Cp_2TiXBn is formed (possibly concertedly). In the final step, eq 18, Cp_2TiXBn reacts in a slow process with another molecule of BnCl to afford bibenzyl, Bn_2, as the final product in accordance with experimental observations.[10c,19]

On the basis of the above reaction scheme, a consistent set of data could be extracted from the best fits as depicted in Figures 5 and 6. The reactions of eqs 13, 15, and 17 were assumed to be fast, so that their only influence on the kinetics would be through the stoichiometry. In contrast, the reaction in eq 18 being slow could be excluded from the kinetic analysis. Furthermore, the rate constant k_{16} was fixed at 0.44 M^{-1} s^{-1} as determined elsewhere.[10c] Attempts to encompass a situation in the simulations where the reactivity of the dimer would be negligible and the monomer with its free coordination site the only reactive species, lowered the quality of the fits.

(19) Control experiments involving benzyl chloride, ZnI_2, and Bu_4NI verified that benzyl chloride would not be converted to benzyl iodide in the Zn-Cp_2TiI_2 solutions.

Table 3. Rate Constants k_{12}, k_{14}, k_{16}, k_{19}, k_{20}, and k_{21} for the Reactions between Ti^{III}-Based Species and Benzyl Chloride or Benzaldehyde Measured in THF at 20 °C[a]

	BnCl			PhCHO		
	k_{12} Cp_2TiX	k_{14} $(Cp_2TiX)_2$	k_{16} Cp_2Ti^+	k_{19} Cp_2TiX	k_{20} $(Cp_2TiX)_2$	k_{21} Cp_2Ti^+
X = Cl[b]	0.66	0.80	0.44	<2	70	
X = Br	0.65	0.60	0.44	5	70	5
X = I	0.60	0.70	0.44	*c*	*c*	*c*

[a] All rate constants are given in units of M^{-1} s^{-1}. [b] From ref 10c. [c] Measurements were irreproducible.

The extracted data are collected in Table 3 along with data obtained previously for Zn-Cp_2TiCl_2. The conclusion is that the reactivities of Cp_2TiX, $(Cp_2TiX)_2$, and Cp_2Ti^+ with rate constants of 0.44−0.80 M^{-1} s^{-1} are largely the same, independent of X. In comparison, it might be mentioned that the reactivity of $Cp_2TiX_2^-$ toward BnCl with rate constants of <0.019, <0.12, and <0.26 M^{-1} s^{-1} for X = Cl, Br, and I, respectively,[10b] is lower, although $Cp_2TiX_2^-$ should be the best electron donor from a thermodynamic point of view. The variation in the $E°$'s of the species concerned (see Table 1) is thus not reflected in the kinetic features, indicating that the reaction of Cp_2Ti^+, in particular, possesses strong inner-sphere character with a substantial stabilization of the transition state. Actually, this does not seem to be an unreasonable interpretation as Cp_2Ti^+ with its positive charge and an easily accessible coordination site would be expected to be capable of interacting with the chlorine atom in benzyl chloride. In this respect, it may seem surprising that $(Cp_2TiX)_2$, having no free coordination site (see structure **II** in Chart 1), should exhibit the same reactivity as Cp_2TiX. However, as discussed elsewhere[10c] the explanation might reside in the fact that the dimer structure in solution is of the half-open type depicted as **III** in Chart 1, as this would facilitate the coordination of benzyl chloride. In line with this interpretation, we attribute the low reactivity of $Cp_2TiX_2^-$ to its lack of a free coordination site.

Benzaldehyde. A series of experiments using different initial concentrations of Zn-Cp_2TiX_2 was carried out on the reactions involving PhCHO. These reactions are of great importance for synthetic purposes, as they present a convenient method for carrying out pinacol couplings to afford vicinal diols[2] as depicted in the generalized reaction sequence shown below.[10c]

The reaction mechanism consists of an initial electron transfer process from Cp_2TiX, eq 19, $(Cp_2TiX)_2$, eq 20, or Cp_2Ti^+, eq 21, to PhCHO followed by dimerization of the thus formed ketyl radicals, eq 22. Note that additional halide transfer from the metal halides is included in eq 21. The kinetic traces recorded for the different solutions of Zn-Cp_2TiBr_2 are shown in Figure 7.

A characteristic feature of these traces is that the contribution from $(Cp_2TiBr)_2$ is largest initially, as its

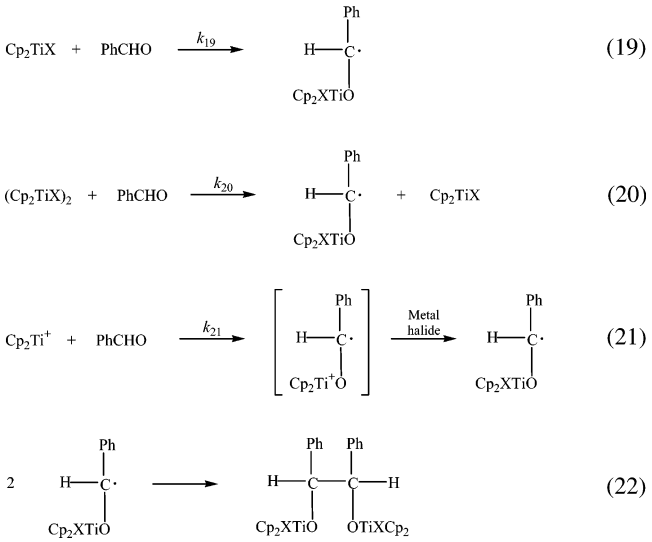

relative concentration under these conditions is high. As the decay proceeds and the overall concentration of the Ti^{III}-based species diminishes, the reactivities of Cp_2TiBr and Cp_2Ti^+ become responsible for the tail of the decay. As seen in Figure 7 reasonable fits can be obtained for the four different concentrations of Zn-Cp_2TiBr_2 employed, allowing the extraction of all three rate constants k_{19}, k_{20}, and k_{21}. In our previous study we attempted to study directly the reaction of Cp_2Ti^+ with PhCHO, but these experiments had to be renounced because of too low reproducibility.[10c] For Zn-Cp_2TiI_2, the overall picture is the same as that for Zn-Cp_2TiBr_2, although the lack of reproducibility prevented us from extracting reliable rate data. Presumably, this failure should be ascribed to the sensitivity of Zn-Cp_2TiI_2 toward the presence of residual water in THF. However, as inferred from the comparison of traces presented for Zn-Cp_2TiBr_2 and Zn-Cp_2TiI_2 in the inset of Figure 7, it may be concluded that the overall reactivity of the latter solution with its higher concentration of Cp_2Ti^+ is slightly lower.

The extracted rate data are gathered in Table 3 along with data obtained previously for X = Cl.[10c] Overall, we find that the reactions of PhCHO are faster than those of BnCl, which is consistent with a larger inner-sphere character in the former case because of the oxophilicity of titanium complexes. The rate constants for Cp_2TiX and $(Cp_2TiX)_2$ are by and large independent of X, despite the differences present in the pertinent potentials (approximately 70 mV, see Table 1). Even Cp_2Ti^+, associated with a high value of $E°$, exhibits the same reactivity as Cp_2TiBr. However, the reactivity of $(Cp_2TiBr)_2$ surpasses that of Cp_2TiBr and Cp_2Ti^+ by a factor of 14. For the Zn-Cp_2TiCl_2 solution the rate difference between $(Cp_2TiCl)_2$ and Cp_2TiCl is found to be even larger, constituting at least a factor of 35.[10c] These results might be interpreted as if the structure of the dimer indeed is of the half-open type **III** with its easily accessible coordination site rather than the symmetric structure **II**.

Diastereoselectivities

The cyclic voltammetric and kinetic investigations indicate that trinuclear complexes (**IV** in Chart 1) are not involved in the electron transfer step in the pinacol coupling reaction of benzaldehyde as shown in eqs 19−21. On the other hand, these results do not provide direct information on the actual coupling step in eq 22, which preferentially leads to the formation of the *dl*-isomer. In the literature three main mechanisms based on product formation studies have been proposed for explaining the diastereoselective outcome of such pinacol couplings of aryl and alkyl aldehydes as shown in Scheme 2.[20] In the first case, coordination of both ketyl oxygens to the same Lewis acidic metal center would promote a pseudo-intramolecular diradical coupling, which in turn leads to the preferential formation of the *dl*-isomer for sterical reasons.[21] The transition state involving trinuclear complexes represents a modification of this mechanism as illustrated in Scheme 3 (with X = Cl).[22] This structure has been proposed in two variants, either as two pentacoordinated Ti^{IV} atoms[2a,i] or as tetracoordinated centers where two of the chlorines from the original trimetallic complex have been substituted by oxygen upon reduction of benzaldehyde to a diketyl intermediate.[2c,d,23]

The second but closely related mechanism in Scheme 2 involves addition of a ketyl radical to a metal-complexed carbonyl species. In the case where the same metal center is implicated, a similar stereochemical preference for the *dl*-isomer would be predicted. Typically, this mechanism has been proposed for intra-

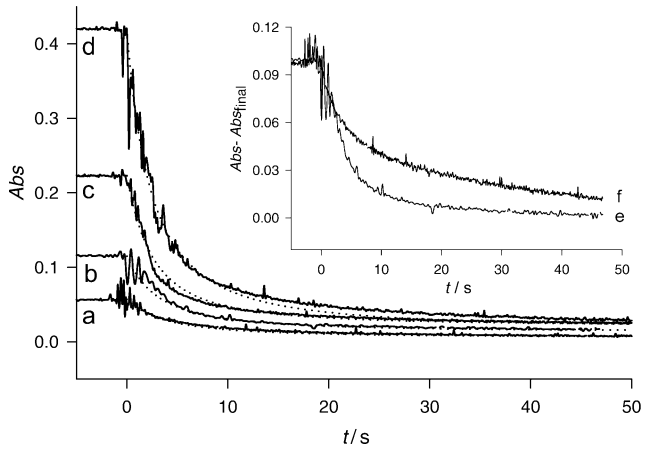

Figure 7. Kinetic traces (absorption vs time) recorded for the decay of Ti^{III} at a wavelength $\lambda = 800$ nm in THF for the reactions of 15 mM PhCHO with (a) 1.0, (b) 2.0, (c) 4.0, and (d) 8.0 mM solutions of Zn-Cp_2TiBr_2. The dotted curves are the best fits based on simulation of eqs 8, 11, and 19−21. Inset: Kinetic traces (absorption vs time) recorded for the decay of Ti^{III} at a wavelength $\lambda = 800$ nm in THF for the reactions of 15 mM PhCHO with 2.0 mM solutions of (e) Zn-Cp_2TiBr_2 and (f) Zn-Cp_2TiI_2. The final absorption, Abs_{final}, has been used as zero point.

(20) For reviews on the pinacol coupling, see: (a) Wirth, T. *Angew. Chem., Int. Ed. Engl.* **1996**, *35*, 61. (b) Dushin, R. G. In *Comprehensive Organometallic Chemistry II*; Hegedus, L. S., Ed.; Pergamon: Oxford, 1995; vol. 12, p 1071. (c) Fürstner, A. *Angew. Chem., Int. Ed. Engl.* **1993**, *32*, 164. (d) Robertson, G. M. In *Comprehensive Organic Synthesis*; Trost, B. M., Ed.; Pergamon: Oxford, 1991; p. 563. (e) McMurray, J. E. *Chem. Rev.* **1989**, *89*, 1513. (f) Kahn, B. E.; Rieke, R. D. *Chem. Rev.* **1988**, *88*, 733.

(21) Hirao, T.; Hatano, B.; Imamoto, Y.; Ogawa, A. *J. Org. Chem.* **1999**, *64*, 7665, and references therein.

(22) Clerici, A.; Clerici, L.; Porta, O. *Tetrahedron Lett.* **1996**, *37*, 3035.

Scheme 2. Mechanisms Proposed for Low-Valent Transition Metal-Promoted Pinacol Coupling Reactions

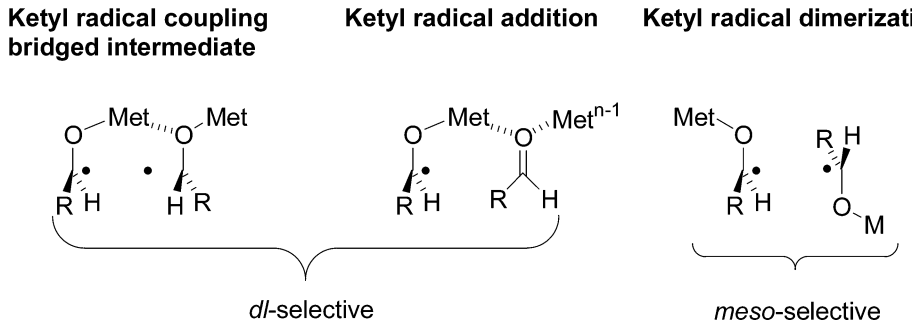

Scheme 3. Mechanism Proposed for the Ti^{III}-Promoted Pinacol Coupling Reactions Involving a Trinuclear Complex

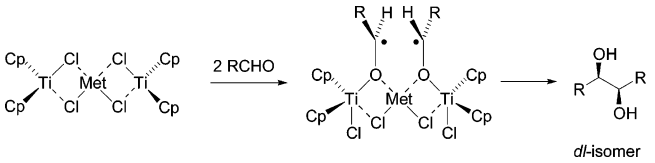

Scheme 4. Mechanism Proposed for the Ti^{III}-Promoted Pinacol Coupling Reactions Involving $(Cp_2TiX)_2$

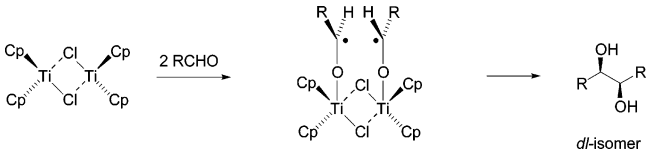

Table 4. Ratios of *dl*:*meso* for the Hydrobenzoin Products Obtained from Stoichiometric Titanocene Halide Promoted Pinacol Couplings of Benzaldehyde in THF[a]

	X = Cl	X = Br	X = I
Zn-Cp_2TiX_2	97:3	94:6	87:13
Mn-Cp_2TiX_2	97:3	95:5	90:10
Al-Cp_2TiX_2	97:3	95:5	91:9
"Cp_2TiX_2 + e"[b]	96:4	94:6	86:14

[a] Ratios were determined by ^1H NMR spectroscopy of the crude reaction mixtures. [b] Electrochemical reduction of Cp_2TiX_2 was carried out in the presence of 0.2 M Bu_4NPF_6.

molecular pinacol couplings to afford cyclic diols.[1b,24,25] Finally, the third mechanism involves the simple bimolecular dimerization of two metal-complexed ketyl radical intermediates to form the pinacolate.[20,23,24d,26] For sterical reasons one would expect that the preferred product obtained from this mechanism is the *meso*-isomer, whereas for the intramolecular pinacol cyclizations to small rings, the major product would be the *trans*-isomer.

To provide further information regarding the mechanism of this Ti^{III}-promoted vicinal diol formation, a study was undertaken to measure the diastereoselectivities of the hydrobenzoins obtained from the pinacol coupling of benzaldehyde mediated by Met-Cp_2TiX_2 and electrochemically reduced Cp_2TiX_2, varying both the reducing metal and the halogen. The *dl*:*meso* ratios are collected in Table 4. These results are supported by an earlier report by Barden and Schwartz, where similar diastereoselectivities were noted for the dimerization of benzaldehyde with a solution of $Cp_2TiCl/(Cp_2TiCl)_2$.[2b]

First of all, it is important to note that on the basis of the mechanistic interpretation outlined in eqs 19−22 the actual coupling step in eq 22 should be independent of whether the active reagent is Cp_2TiX, $(Cp_2TiX)_2$, or Cp_2Ti^+. This assumption is reinforced by the observation that the same diastereoselectivity is obtained no matter if the electrochemical or metal-based approaches are employed and, furthermore, no matter if the latter procedure is carried out under catalytic or stoichiometric conditions.[1] These results also emphasize that the introduction of any complexes involving a second metal such as the mechanistic proposal in Scheme 3 is not required in order to explain the high *dl*:*meso* ratios. On the other hand, we do see a decrease in the selectivity when the halogen is changed from Cl to Br and I.

Interestingly, in a 2001 paper examining the stereoselectivities of Ti^{III}-promoted pinacol couplings, Dunlap and Nicholas proposed a mechanism where the coupling reaction proceeds through a dimeric structure as shown in Scheme 4,[2i] since this complex would also lead to the formation of the *dl*-isomer. Although this possibility cannot be excluded, the structure contains pentacoordinated Ti^{IV} atoms, which are not very likely considering that species such as Cp_2TiCl_2,[27] $(Cp_2TiCl)_2$,[28] $(Cp_2TiCl)_2MgCl_2$,[29] $(Cp_2TiCl)_2MnCl_2$,[12b] $(Cp_2TiCl)_2ZnCl_2$,[12a] $Cp_2TiCl(OMe)$,[30] and $Cp_2TiCl(OEt)$[31] all exhibit distorted tetrahedral coordination around the Ti cores. In addition, the cyclic voltammetric studies indicated that the mechanism for the electrochemical oxidation of $(Cp_2TiX)_2$ included a fast fragmentation of $(Cp_2TiX)_2^+$, and it would seem unlikely that such a cleavage reaction should not occur even faster when a ketyl radical anion

(23) Yamamoto, Y.; Hattori, R.; Miwa, T.; Nakagai, Y.-I.; Kubota, T.; Yamamoto, C.; Okamoto, Y.; Itoh, K. *J. Org. Chem.* **2001**, *66*, 3865.
(24) (a) Freudenberger, J. H.; Konradi, A. W.; Pedersen, S. F. *J. Am. Chem. Soc.* **1989**, *111*, 8014. (b) Konradi, A. W.; Kemp, S. J.; Pedersen, S. F. *J. Am. Chem. Soc.* **1994**, *116*, 1316, and references therein. (c) Kang, M.; Park, J.; Konradi, A. W.; Pedersen, S. F. *J. Org. Chem.* **1996**, *61*, 5528. (d) Yamamoto, Y.; Hattori, R.; Itoh, K. *J. Chem. Soc., Chem. Commun.* **1999**, 825.
(25) (a) Molander, G. A.; Harris, C. R. *Chem. Rev.* **1996**, *96*, 307. (b) Steel, P. G. *J. Chem. Soc., Perkin Trans. 1* **2001**, 2727.
(26) (a) Pedersen, H. L.; Christensen, T. B.; Enemærke, R. J.; Daasbjerg, K.; Skrydstrup, T. *Eur. J. Org. Chem.* **1999**, *565*, 5. (b) Christensen, T. B.; Riber, D.; Daasbjerg, K.; Skrydstrup, T. *J. Chem. Soc, Chem. Commun.* **1999**, 2051. (c) Riber, D.; Hazell, R. G.; Skrydstrup, T. *J. Org. Chem.* **2000**, *65*, 5382, and references therein.
(27) Clearfield, A.; Warner, D. K.; Saldarriaga-Molina, C. H.; Ropal, R. *Can. J. Chem.* **1975**, *53*, 1622.
(28) Jungst, R.; Sekutowski, D.; Davis, J.; Luly, M.; Stucky, G. *Inorg. Chem.* **1977**, *16*, 1645.
(29) Stephan, D. W. *Organometallics* **1992**, *11*, 996.
(30) Gibson, D. H.; Ding, Y.; Mashuta, M. S.; Richardson, J. F. *Acta Crystallogr.* **1996**, *C52*, 559.
(31) Huffman, J. C.; Moloy, K. G.; Marsella, J. A.; Caulton, K. G. *J. Am. Chem. Soc.* **1980**, *102*, 3009.

Scheme 5. Newman Projections of Possible Conformers Being Responsible for the Products Formed in the Dimerization of Two Ti^{IV}-Bound Ketyl Radicals

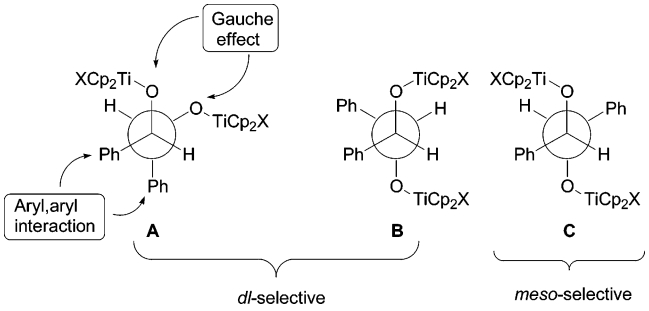

is bound to the Ti^{IV} core.[10b] Finally, electrochemical studies with Cp_2TiX_2 in the presence of excess halide salts have failed to reveal the presence of the pentavalent $Cp_2TiX_3^-$ species.

On the basis of the above discussion it appears most likely that the coupling step in the titanocene halide promoted pinacol couplings proceeds via the dimerization of two Ti^{IV}-bound ketyl radicals in line with the third mechanistic proposal of Scheme 2. Previously, this has also been suggested by Barden and Schwartz.[2b] However, the experimental finding that the major product is the *dl*- rather than the expected *meso*-isomer and that there is a small but evident drop observed in diastereoselectivity when the halogen is changed from Cl to Br and I underlines the importance of the exact nature of the titanocene moiety. The question remains whether this can be attributed to a sterical or possibly an electronic effect in the dimerization step or as a combination of the two effects.

To provide a plausible explanation, which also takes into consideration the halogen effect, we have examined in Scheme 5 the three two-dimensional Newman projections **A**, **B**, and **C** of two approaching $TiCp_2X$-bound ketyl radicals in the intermolecular dimerization. On the basis of purely sterical reasons, **C** leading to the *meso*-product would seem the most likely candidate, as it clearly must possess the least sterical interactions between the nearing substituents. However, this is contradicted by the experimental observations, suggesting that this transition structure is essentially absent. Instead, we propose that electronic effects may be playing an important role in the coupling step. Examination of the Newman projections **A** and **B** reveals that both possess two aryl groups in a *gauche* relationship, which potentially could provide for an energetically favorable aryl−aryl interaction.[32] Whereas this cannot account for the halogen effect observed for these reactions, structure **A** reveals an alternative *gauche* effect between two electronegative substituents, namely that of the two Ti^{IV}-alkoxides. Previously, it has been shown that such a stereoelectronic effect can favor a *gauche* conformation by as much as 1 kcal mol^{-1} for vicinal fluorine and oxygen substitutents.[33] Although speculative, it could be expected that an increase in the electronegativity of the $OTiCp_2X$ substituents would occur in the direction going from X = I to Cl. The *gauche* effect would hence be greatest for X = Cl, thereby suggesting that projection **A**, which leads to the *dl*-diol, might be a main contender in the C−C bond forming process. It should be noted that the small differences found for the diastereoselectivities upon exchanging the halogens in the Ti^{III}-based species would correspond to a variation in the *gauche* effect of less than 1 kcal mol^{-1}.

Some support for this hypothesis can be found in the recent work reported from the Itoh group investigating the ability of Cp_2TiPh to promote inter- and intramolecular pinacol coupling of aldehydes.[23] In conjunction with our hypothesis, it can be expected that the electronegativity of the $OTiCp_2Ph$ substituent is less than that of the corresponding halogen-containing species. Hence, the diastereoselective outcome of this coupling reaction would also be expected to be lower than for the $OTiCp_2X$ substituent. And indeed, a *dl*:*meso* ratio of 67:33 was observed for the benzohydroin product obtained using Cp_2TiPh as the reducing agent.

Although sterical effects should not be excluded, the *gauche* effect in pinacol couplings involving ketyl radical dimerization with noncoordinating metal centers could play an important role in dictating the stereochemical outcome of the reaction products. Further work will have to be carried out to confirm the role of this stereoelectronic effect in pinacol coupling reactions.[34]

Conclusions

The identity of Ti^{III} species generated in THF by Zn-based reduction of Cp_2TiX_2 (X = Cl, Br, and I) has been clarified by means of cyclic voltammetry and kinetic measurements. It is found that the principal species formed are a mixture of Cp_2TiX, $(Cp_2TiX)_2$, and Cp_2Ti^+, the distribution of which is dependent on the halogen considered. Interestingly, Cp_2Ti^+ is present in quite substantial amounts only for X = Br and I, whereas it is completely absent for X = Cl. In all three solutions the amounts of Cp_2TiX and $(Cp_2TiX)_2$ are appreciable, being formed in a mixture having a dimerization equilibrium constant of $(1-3) \times 10^3$ M^{-1}. The latter parameter is independent of the metal (Zn, Mn, or Al) and halogen considered, although the dimerization rate constant is 10−25 times larger for X = Br and I than for X = Cl. Standard potentials determined through simulations of the cyclic voltammograms increase for the identified redox couples in the order $Cp_2TiX_2/Cp_2TiX_2^- \ll (Cp_2TiX)_2^+/(Cp_2TiX)_2 < Cp_2TiX^+/Cp_2TiX \ll Cp_2Ti^{2+}/Cp_2Ti^+$. For a given halogen-containing Ti^{III} species a small increase in the standard potentials is seen going from X = Cl to Br and I. From a thermodynamic point of view $Cp_2TiX_2^-$ is thus expected to be the strongest electron donor among the different Ti^{III} species with the halogen effect increasing the electron-donating ability in the order I < Br < Cl. However, on the basis of kinetic measurements the reactivity of $(Cp_2TiX)_2$ is found to be larger than or comparable to the reactivities

(32) Tsuzuki, S.; Honda, K.; Uchimaru, T.; Mikami, M.; Tanabe, K. *J. Am. Chem. Soc.* **2002**, *124*, 104.

(33) For discussion of the electronic gauche effect, see (a) Wolfe, S. *Acc. Chem. Res.* **1972**, *5*, 102. (b) Senderowitz, H.; Golender, L.; Fuchs, B. *Tetrahedron* **1994**, *50*, 9707. (c) Senderowitz, H.; Fuchs, B. *THEOCHEM* **1997**, *395/396*, 123. (d) Craig, N. C.; Chen, A.; Suh, K. H.; Klee, S.; Mellau, G. C.; Winnewisser, B. P.; Winnewisser, M. *J. Am. Chem. Soc.* **1997**, *119*, 4789. (c) Ganguly, B.; Fuchs, B. *J. Org. Chem.* **2000**, *65*, 558.

(34) DFT calculations are intended to be carried out to examine the influence of the *gauche* effect on the transition state structure of the dimerization process.

of Cp_2TiX and Cp_2Ti^+ (and much larger than for $Cp_2TiX_2^-$) as assessed in their reactions with benzyl chloride and benzaldehyde. In addition, the rate data are essentially independent of the halogen. Analysis of the diastereoselectivities observed for the hydrobenzoin formation in the titanocene chloride promoted pinacol coupling of benzaldehyde shows a high *dl:meso* ratio of 97:3 with a decreasing trend when X is changed from Cl to Br and I. This effect is explained by means of a *gauche* effect in terms of increased stereoelectronic interactions between the titanocene moieties in the developing Ti^{IV}-bound pinacolate of the transition state. All of the reactions studied in this work, in particular those involving benzaldehyde, proceed by inner-sphere electron transfer pathways.

Experimental Section

Materials. Most chemicals were of commercial origin unless otherwise noted. Benzyl chloride and benzaldehyde were vacuum distilled before use. THF was distilled over sodium and benzophenone under an atmosphere of dry nitrogen. Argon (99.99% purity) was passed through a column of P_2O_5 (Sicapent). Tetrabutylammonium hexafluorophosphate, Bu_4NPF_6, was prepared from a hot aqueous solution containing tetrabutylammonium hydrogen sulfate and potassium hexafluorophosphate. The precipitate was filtered and recrystallized from ethyl acetate and pentane. Tetrabutylammonium iodide was recrystallized twice using THF, dried under vacuum at 60 °C for 24 h, and stored in a glovebox. All handling of it had to take place in a dry atmosphere because of its hygroscopic properties. Bis(cyclopentadienyl)titanium dibromide, Cp_2TiBr_2, was prepared by adding 1.1 equiv of a BBr_3/CH_2Cl_2 solution to Cp_2TiCl_2 dissolved in CH_2Cl_2. Upon 15 min of stirring the solution was evaporated. The red-brown residue was dissolved in CH_2Cl_2, and after filtration this solution was evaporated as well. The product was dried under vacuum at 20 °C for 3−4 h.[35] Bis(cyclopentadienyl)titanium diiodide, Cp_2TiI_2, was synthesized using the same procedure as described for Cp_2TiBr_2 replacing BBr_3 by BI_3. The Zn- and Mn-Cp_2TiX_2 solutions were prepared by adding THF to a flask thoroughly flushed with argon and containing Cp_2TiX_2 besides excess metal. The solutions were stirred for 30 min until a turquoise green color had become apparent. For preparing Al-Cp_2TiX_2 activation of the aluminum foil using $Hg(NO_3)_2$ in THF was required. The activated foil was washed three times with THF before use.

Apparatus. Most of the electrochemical equipment was home-built, and a description of the experimental setup is provided in ref 36. The working electrode was a glassy carbon disk of diameter 1 mm. The electrode surface was polished using 0.25 μm diamond paste (Struers A/S) followed by cleaning in an ethanol bath. The counter electrode was a platinum coil melted into glass, while the reference electrode consisted of a silver wire in a Pyrex glass tube (diameter = 7 mm) containing 0.02 M Bu_4NI + 0.2 M Bu_4NPF_6/THF. The tube was closed at one end by a porous ceramic material (TZ, Export Technishe Keramik, München). All potentials were reported versus the ferrocenium/ferrocene (Fc^+/Fc) redox couple, the potential of which was measured to be 0.52 V vs SCE in 0.2 M Bu_4NPF_6/THF. All handling of chemicals was performed on a vacuum line, and at no point during the different operations was the interference of oxygen allowed. The ohmic drop was compensated with a positive feedback system incorporated in the potentiostat. The kinetic traces were recorded by means of a fiber-optic spectrometer, model S1000 (dip-probe), from Ocean Optics, using a light path length of 1 cm.

Procedure. In the cyclic voltammetric experiments 0.77 g of Bu_4NPF_6 (2.0 mmol) and a small magnetic bar were added to the electrochemical cell. The cell was closed and flushed thoroughly with argon for 10 min. Typically, 9 mL of freshly distilled THF and 1 mL of the appropriate standard solution containing the compound of interest were added to the cell using a syringe, and the solution was stirred for 30 s. All experiments in a series were repeated in order to check the stability of the solution. Special care must be taken when recording voltammograms of the Met-Cp_2TiX_2 solutions, since the metal ions present may be reduced at low potentials and cause deleterious adsorption of metal on the electrode surface. In general, potentials below −1.4 V vs Fc^+/Fc should be avoided. At the end of each series of experiments a small amount of ferrocene was added, and the potential of the Fc^+/Fc couple was measured.

In the kinetic experiments, the UV−vis dip-probe was mounted vertically in a two-necked cell containing a small magnetic bar.[36] The cell was closed and flushed with argon for 10 min before 9 mL of freshly distilled THF was added. From a standard solution containing the appropriate Met-Cp_2TiX_2 typically 1 mL was transferred to the cell. Benzyl chloride or benzaldehyde was added in excess, while the solution was stirred vigorously. The decay of Ti^{III} at the wavelength λ = 800 nm and the concomitant buildup of Ti^{IV} at λ = 535 nm were followed. In the kinetic analysis it was assumed that the extinction coefficients ϵ for the different Ti^{III} ($\epsilon \approx 50$ and 45 M^{-1} cm^{-1} for X = Br and I, respectively) and Ti^{IV} species ($\epsilon \approx 400$ and 700 M^{-1} cm^{-1} for X = Br and I, respectively) would be the same. In comparison, the corresponding values for X = Cl are $\epsilon \approx 45$ and 200 M^{-1} cm^{-1}, respectively.

The diastereoselectivities obtained in the pinacol coupling reactions between benzaldehyde and a stoichiometric amount of the Ti^{III}-containing species were after acidic workup determined by ^1H NMR spectroscopy.[2b]

Acknowledgment. The Danish Natural Science Research Council is thanked for financial support.

Supporting Information Available: Text giving a description of the model parameters used in the simulations and a compilation of cyclic voltammograms of Zn-Cp_2TiX_2 along with relevant fits. This material is available free of charge via the Internet at http://pubs.acs.org.

OM049257M

(35) Druce, P. M.; Kingston, B. M.; Lappert, M. F.; Spalding, T. R.; Srivastava, R. C. *J. Chem. Soc. A* **1969**, 2106.

(36) Pedersen, S. U.; Christensen, T. B.; Thomasen, T.; Daasbjerg, K. *J. Electroanal. Chem.* **1998**, *454*, 123.